

Signals, Concepts, and Laws: Toward Universal, Explainable Time-Series Forecasting

Hongwei Ma, Junbin Gao, Minh-ngoc Tran
 The University of Sydney
 hongwei.ma@sydney.edu.au

Abstract

Accurate, explainable and physically credible forecasting remains a persistent challenge for multivariate time-series with domain-varying statistical properties. We propose DORIC, a Domain-Universal, ODE-Regularized, Interpretable-Concept Transformer for Time-Series Forecasting that generates predictions through five self-supervised, domain-agnostic concepts while enforcing differentiable residuals grounded in first-principles constraints. **The concepts are softly regressed toward analytic statistics of the raw signal, and a driven-damped ODE head couples these concepts to the forecast as a shared, mean-reverting dynamical template across datasets.** Unlike prior efficiency-focused Transformers, such as Informer(sparse attention) or FEDformer(frequency priors), DORIC combines latent explainability with explicit scientific constraints, while preserving the attention mechanism’s capacity to model long-range dependencies. We evaluate DORIC on six publicly-available datasets and it achieves the lowest error in eight of twelve MSE/MAE metrics. Compared with TimeMixer, DORIC outperforms it on four datasets while maintaining strong interpretability. **Interpretability analyses show that the learned concepts remain strongly aligned with their analytic targets, physics residuals stay relative to the signal scale, and the learned ODE coefficients follow domain-consistent patterns.** Ablation studies reveal complementary contributions: removing the physics residual increases average MSE from 0.328 to 0.547, eliminating concept alignment raises it to 0.698, and replacing the shared encoder with disjoint concept heads results in a 76% increase.

1 Introduction

Real-world decision systems, from power-grid dispatch and urban mobility control to epidemic surveillance and high-frequency trading, depend on fast, accurate, and trustworthy forecasts of multivariate time-series. Classical linear models, exemplified by the Box-Jenkins ARIMA methodology (Tunncliffe Wilson, 2016), provide statistical rigor but struggle with high-frequency, non-stationary data or dynamics governed by latent physical constraints. Over the past decade, attention-based deep learning has revolutionized sequential modelling: the Transformer architecture introduced by Vaswani et al. (2017) replaced recurrence

with self-attention, enabling parallel learning over long-contexts. Subsequent efficiency-oriented variants, such as Reformer (Kitaev et al., 2020) and Log-Trans (Li et al., 2019), reduce memory overhead via locality-sensitive hashing and log-sparse kernels. Meanwhile, domain-specific advances, such as In-former (Zhou et al., 2021), Autoformer (Wu et al., 2021), and FEDformer (Zhou et al., 2022), introduced decomposition, auto-correlation and frequency sparsity to enhance long-horizon accuracy. More recently, PatchTST (Nie et al., 2023b) demonstrated further gains via patching and exponential-smoothing priors. A comprehensive survey (Wen et al., 2023) attests to the field’s explosive growth. Despite these advancements, three structural gaps remain.

- **Gap 1 – Physics non-compliance.** Purely data-driven Transformers can produce trajectories that violate fundamental constraints (e.g., mass-balance or energy conservation), thereby undermining stakeholder trust and limiting deployment in safety-critical domains.
- **Gap 2 – Latent opacity.** Although post-hoc explanation methods exist, their fidelity degrades in multivariate settings. In contrast, concept-driven transparency pioneered by Concept Bottleneck Models (Koh et al., 2020) and their stochastic extensions (Vandenhirtz et al., 2024) remains under-explored in the context of time-series forecasting.
- **Gap 3 – Lack of universality.** Most specialised architectures are tailored to specific domains (e.g., weather or finance) and struggle to generalise across varying sampling rates, noise characteristics, and seasonality patterns.

To bridge these gaps, we view long-horizon forecasting through an *interpretability-first* lens. Rather than adding ever more opaque modules, we ask whether a single concept–physics layer can serve as a reusable interface between diverse multivariate time series and human experts. Concretely, we introduce **DORIC**, a forecasting architecture that augments a standard encoder with (i) a small set of physically motivated concepts computed from the input signals, and (ii) a physics-informed head that couples these concepts via simple laws. This yields a model whose internal “dials” have stable semantics across datasets while remaining competitive with strong baselines.

Contributions. The contributions of this work are threefold:

- **A universal concept–physics layer for multivariate time series.** We design five low-level yet broadly applicable concepts (level, velocity, instantaneous power, dominant periodic amplitude, and local volatility) that can be attached to standard sequence encoders. These concepts are computed by causal statistics and serve as a shared vocabulary across datasets, rather than being tailored to any single benchmark.
- **A physics-informed head with provable training dynamics.** We couple the concepts to the forecast through a driven–damped first-order ODE and

turn this ODE into algebraic residuals. The resulting physics loss admits a ramp-up schedule under which SGD converges while the physics violation vanishes. This connects the training trajectory to a clear three-stage story: feasibility (physics residual collapse), concept alignment, and data fit.

- **An interpretability-first evaluation of forecasting performance.** We show on seven standard benchmarks that plugging the concept–physics layer into a strong Transformer backbone achieves accuracy comparable to recent state-of-the-art models, while enabling concept-level analyses, gradient-based local sensitivities, and cross-dataset comparisons. Ablations demonstrate how concept supervision and physics penalties jointly control the trade-off between predictive accuracy and interpretability.

Scope of interpretability and scientific value. Our interpretability claim is scoped at the level of the shared bottleneck and dynamical template rather than at every individual weight in the network. Each forecast \hat{y}_t is required to pass through a five-dimensional concept vector $c_t = (c_{1,t}, \dots, c_{5,t})$ and a driven–damped ODE head that are shared across all datasets. These coordinates are not arbitrary hidden units: they are softly regressed towards analytic statistics of the raw signal (sliding mean, local velocity, instantaneous power, dominant periodic amplitude, local volatility), so that the bottleneck remains tied to physically meaningful quantities instead of drifting into opaque features. The ODE head then combines these concepts through a mean-reverting dynamics that is also shared across domains. Together, this design yields a mediating mechanism from past observations to future predictions: time points influence the forecast only through how they shape the concept trajectories and how those trajectories are processed by the ODE. We do not claim that these five concepts exhaust all possible explanations, but that DORIC enforces a low-dimensional, physically anchored interface that is consistent across heterogeneous time-series domains.

2 Literature Review

Early time-series forecasting relies on stochastic linear models such as the Box–Jenkins ARIMA (Tunncliffe Wilson, 2016), whose identification–estimation–diagnosis cycle remains influential but often fails under the non-stationarity of modern telemetry.

Deep learning models capture time-series patterns with specifically-designed architectures spanning a wide range of foundation backbones, including CNNs (Wang et al., 2023; Wu et al., 2023; Hewage et al., 2020), RNNs (Lai et al., 2018; Qin et al., 2017; Salinas et al., 2020), Transformers (Vaswani et al., 2017) and MLPs (Zeng et al., 2023b; Zhang et al., 2022; Oreshkin et al., 2019; Challu et al., 2023). The quadratic cost of vanilla attention spurred efficient variants, Reformer (Kitaev et al., 2020) and LogTrans (Li et al., 2019), and domain-specific advances: Informer’s ProbSparse attention (Zhou et al., 2021), Autoformer’s trend–seasonality decomposition (Wu et al., 2021), FEDformer’s Fourier sparsity (Zhou et al., 2022), PatchTST’s patch-token strategy (Nie et al., 2023b),

and TimeMixer (Wang et al., 2024). A 2023 survey (Wen et al., 2023) documents more than 120 Transformer adaptations for time-series forecasting.

Despite these advances, interpretability remains a challenge, prompting growing interest in concept-level supervision. Concept Bottleneck Models (Koh et al., 2020) demonstrate that forcing predictions through human-meaningful variables can maintain accuracy while enabling user interventions. Stochastic CBMs (Vandenhirtz et al., 2024) generalized this idea by modelling concept dependencies probabilistically. FF Bottleneck (van Sprang et al., 2025) used an AR model as a surrogate concept within a Transformer architecture; however, empirical results revealed that the standalone AR model outperformed FF Bottleneck on four out of the six datasets.

In parallel, physics-informed learning has emerged as a remedy for physically implausible outputs. Raissi’s PINNs framework (Raissi et al., 2019) pioneered the joint optimization of data and governing equations; PGTransNet (Wu et al., 2024) integrated physics-guided self-attention for Pacific-Ocean temperature forecasting, while physics-informed LSTM variants have been applied to power-transformer health monitoring (Lei et al., 2025). The PhysicsSolver (Zhu et al., 2025) further attests to the potential of incorporating scientific priors into deep learning architectures.

Hybrid work now marries physics with deep networks: a TCN–TFT ensemble improves probabilistic wind forecasts (Mi et al., 2025), while energy-constrained diffusion Transformers extend long-horizon accuracy (Ren et al., 2024). Interpretability has advanced through Temporal Fusion Transformer’s gating and variable-selection (Lim et al., 2021) and through sparse-attention schemes such as Adversarial Sparse Transformer (Wu et al., 2020) and Query-Selector attention (Klimek et al., 2022). Complementing advances in model architecture, evaluation paradigms have matured: GraphCast — a graph-neural extension that outperforms ECMWF simulations on 90% of medium-range weather targets (Lam et al., 2023) — demonstrates that ML systems can rival numerical solvers at global scale. Meanwhile, foundation models like TimeGPT (Garza et al., 2024) deliver strong zero-shot generalization capabilities across diverse time-series domains. Nevertheless, critical evaluations have shown that simple linear baselines can outperform many Transformer variants when evaluated rigorously, as highlighted in the “Are Transformers Effective for Time-Series Forecasting?” paper (Zeng et al., 2023a). Additionally, the rise of diffusion-based Transformers (Fu et al., 2025) reflects the field’s continued pursuit of the right balance between model complexity and effective inductive biases.

In summary, although current approaches span efficiency improvements, frequency-domain finesse, multiresolution structure and physics-guided regularization, no existing model simultaneously guarantees physical plausibility, concept-level transparency and cross-domain universality. DORIC fills this gap by fusing a novel five-concept bottleneck with analytic residual constraints inside a Transformer backbone and validating its effectiveness across six heterogeneous benchmarks.

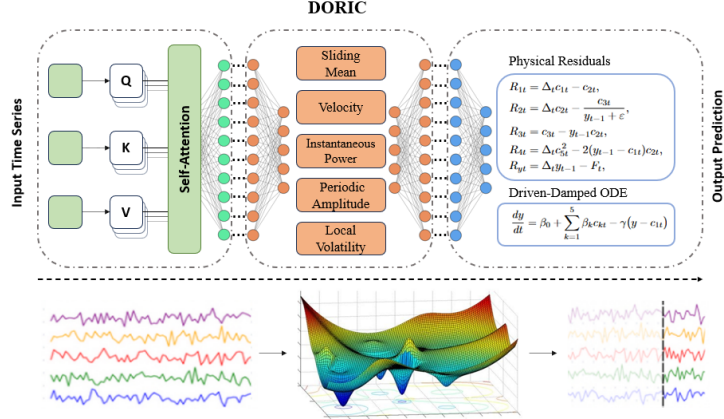


Figure 1: DORIC Structure

3 Methodology

This section introduces the methodology of DORIC. The overall architecture of DORIC is illustrated in Figure 1, time series data first enters the transformer encoder, then undergoes conceptual layer transformation and physical layer constraints, and finally generates a prediction..

3.1 Raw Data and Forecasting Goal

We start from a single-channel time series

$$\mathbf{y}_{1:T} = (y_1, y_2, \dots, y_T) \in \mathbb{R}^T \quad (1)$$

where $T \in \mathbb{N}$ denotes the experiment length (e.g., $T = 24000$ for three years of hourly data), and y_t is the raw observation at discrete time index t in its original physical unit.

At forecast step $t (> L)$ we reveal the strictly causal window

$$\mathbf{y}_{t-L:t-1} = (y_{t-L}, \dots, y_{t-1}) \in \mathbb{R}^L, \quad L \geq \tau + 1, \quad (2)$$

where L is the look-back horizon (e.g. $L = 120$ for five days for hourly or five months for daily-weekly signals), and τ is the conceptual sub-window used later in equation (10), e.g. $\tau = 50$.

Our forecasting operator is therefore a map

$$f_{\Theta} : \mathbb{R}^L \longrightarrow \mathbb{R}, \quad \hat{y}_t = f_{\Theta}(\mathbf{y}_{t-L:t-1}), \quad (3)$$

where Θ collects all trainable parameters of the network (weights, biases, and physics coefficients).

3.2 The Causal Transformer Encoder

The encoder converts the raw window, denoted by $\mathbf{y}_{t-L:t-1}$, into a dense vector $\mathbf{z}_t \in \mathbb{R}^d$, where d is the dimension of the latent embedding, summarizing all past information. The encoder consists of the following layers:

3.2.1 Initial Token Embedding:

Let

$$\mathbf{H}^{(0)} = \underbrace{\mathbf{y}_{t-L:t-1} \mathbf{W}_e}_{\text{value} \rightarrow \text{vector}} + \underbrace{\mathbf{P}}_{\text{position}}, \quad (4)$$

where $\mathbf{W}_e \in \mathbb{R}^{1 \times d}$ (row) is the embedding matrix, mapping each scalar value to a d dimensional vector, $\mathbf{P} \in \mathbb{R}^{L \times d}$ encodes absolute positions via sinusoidal basis: $P_{i,2k} = \sin(i/10^{4k/d})$, $P_{i,2k+1} = \cos(i/10^{4k/d})$, and $\mathbf{H}^{(0)} \in \mathbb{R}^{L \times d}$ is the initial token matrix.

3.2.2 Masked Multi-Head Attention:

We stack N_L Transformer blocks: each block applies

$$\mathbf{H}^{(\ell)} = \text{LN}\left(\mathbf{H}^{(\ell-1)} + \text{MHA}(\mathbf{H}^{(\ell-1)})\right), \ell = 1, \dots, N_L. \quad (5)$$

where LN is the pre-norm layer normalization, and MHA is the masked multi-head attention,

The masked multi-head operator MHA with H heads is defined as,

$$\text{MHA}(\mathbf{H}) = \left[\bigoplus_{h=1}^H (\alpha^h \mathbf{V}^h) \right] \mathbf{W}_o, \quad (6)$$

$$\alpha^h = \text{softmax}\left(\frac{1}{\sqrt{d}} \mathbf{Q}^h \mathbf{K}^{h\top} + \mathbf{M}\right). \quad (7)$$

3.2.3 Latent History Vector:

From the output of the final block $\mathbf{H}^{(N_L)}$, we take the token at the last position L as the latent embedding, denoted by

$$\mathbf{z}_t = \mathbf{H}_L^{(N_L)} \in \mathbb{R}^d. \quad (8)$$

Due to the global receptive field of attention, \mathbf{z}_t already contains information from all other L positions.

3.3 The Concept Bottleneck Layer g_ϕ

The latent vector \mathbf{z}_t is then compressed into a five-dimensional code that can be directly supervised using domain knowledge. In this layer, we use the following three steps to form the concept information.

3.3.1 Learning Concepts:

To form the five context concepts, we use a two-layer MLP, as defined below

$$\mathbf{c}_t = g_\phi(\mathbf{z}_t) = \mathbf{W}_2 \sigma(\mathbf{W}_1 \mathbf{z}_t + \mathbf{b}_1) + \mathbf{b}_2, \quad \mathbf{c}_t \in \mathbb{R}^5, \quad (9)$$

where $\sigma(\cdot)$ is the ReLU activation, the connecting weights $\mathbf{W}_1 \in \mathbb{R}^{d_1 \times d}$ and $\mathbf{W}_2 \in \mathbb{R}^{5 \times d_1}$, and the bias $\mathbf{b}_1 \in \mathbb{R}^{d_1}$ and $\mathbf{b}_2 \in \mathbb{R}^5$. Denote all the learnable parameters by $\phi = \{\mathbf{W}_1, \mathbf{b}_1, \mathbf{W}_2, \mathbf{b}_2\}$.

This bottleneck constrains the model to transmit all information through just five real-valued variables, ensuring that any downstream decision depends solely on these quantities, and making them fully inspectable and interpretable.

3.3.2 Analytical Soft Targets:

We endow those five coordinates with physical meaning through soft targets generated by causal statistics:

$$\mathbf{c}_t^* = (c_{1t}^*, \dots, c_{5t}^*), \quad (10)$$

We denote by y_t the target series at time t and by $X_t \in \mathbb{R}^N$ the full multivariate input at time t . From each history segment $y_{t-\tau:t-1}$ we derive a vector of *concept targets* $c_t^* = (c_{1,t}^*, \dots, c_{5,t}^*) \in \mathbb{R}^5$ using simple causal statistics. These c_t^* serve as *soft targets* for the concept predictor $g_\phi \circ f_\theta$; the network is not forced to exactly reproduce every statistic, but is nudged toward interpretable regions of the feature space.

$$\begin{aligned} c_{1t}^* &= \frac{1}{\tau} \sum_{s=t-\tau}^{t-1} y_s && \text{(sliding mean),} \\ c_{2t}^* &= y_{t-1} - y_{t-2} && \text{(velocity),} \\ c_{3t}^* &= y_{t-1} c_{2t}^* && \text{(instantaneous power),} \\ (a_1, b_1) &:= DFT_1(y_{t-\tau:t-1} - c_{1t}^*), \\ c_{4t}^* &= 2\sqrt{a_1^2 + b_1^2} && \text{(dominant periodic amplitude),} \\ c_{5t}^* &= \sqrt{\frac{1}{\tau} \sum_{s=t-\tau}^{t-1} (y_s - c_{1t}^*)^2} && \text{(local volatility).} \end{aligned} \quad (11)$$

where DFT_1 extracts the first Fourier coefficient on the window and a_1, b_1 are the cosine and sine components, respectively. Every summation index stops at $t-1$; no future value is ever used, maintaining on-line deployability.

Rather than assigning a separate semantic label to every time index, DORIC explains forecasts through the evolution of a small set of shared concepts and their contributions in the ODE head. Individual time points influence the prediction only via how they update the concepts, which we argue is a more stable and transferable interface than attempting to label every y_t directly.

Notation for concepts and soft targets. At each time t we have a five-dimensional concept vector $c_t = (c_{1,t}, \dots, c_{5,t}) \in \mathbb{R}^5$ and an analytic “soft target” $c_t^* = (c_{1,t}^*, \dots, c_{5,t}^*) \in \mathbb{R}^5$ defined by Eqs. (10)–(11). We use the following convention:

- $c_{1,t}$ (*level*): sliding mean of y over a causal window of length τ ;
- $c_{2,t}$ (*growth*): local velocity (finite difference of the level);
- $c_{3,t}$ (*instantaneous power*): local energy, proportional to y_t^2 ;
- $c_{4,t}$ (*dominant periodic amplitude*): magnitude of the leading seasonal harmonic in the window;

- $c_{5,t}$ (*local volatility*): standard deviation of the detrended signal over the same window.

3.3.3 Concept Alignment Loss:

The concept alignment loss then penalizes deviations between the predicted concepts $c_t = g_\phi(f_\theta(X_{t-L+1:t}))$ and the causal statistics c_t^* :

$$\mathcal{L}_{\text{concept}} = \frac{1}{N} \sum_{i=1}^N \sum_{t=L+1}^T \|c_{i,t} - c_{i,t}^*\|_2^2. \quad (12)$$

We treat c_t^* as *soft* supervision rather than hard constraints. This makes the model robust to missing values, noise, and cross-column heterogeneity, and lets the network adjust the effective window length and weighting within each statistic when this yields better data fit without destroying the interpretability of each concept.

3.4 The Physics-Informed Head h_ψ

Having isolated five interpretable dials, we now impose a *first-principles* relationship between the predicted value \hat{y}_t and the concepts. We break it down into three components.

3.4.1 Driven-damped ODE:

$$\frac{dy}{dt} = \beta_0 + \sum_{k=1}^5 \beta_k c_{kt} - \gamma(y - c_{1t}), \quad (13)$$

where

- β_0 — constant baseline drift,
- β_k — coupling weights (to be learned) connecting each concept c_{kt} to the change rate of y ,
- $\gamma > 0$ — relaxation speed driving y towards its local level c_{1t} .

Equation (13) resembles a driven-damped first-order ODE: the concepts supply the drive, and γ supplies the damping.

Role of the ODE template. Importantly, we do not assume that the data-generating process is exactly governed by the linear driven-damped ODE. Instead, the ODE acts as a shared, high-level dynamical template that biases the one-step forecaster h_ψ towards mean-reverting, concept-driven behaviour. The residual $R_y(t)$ measures the inconsistency between the prediction and this template and enters the loss as a soft penalty, rather than a hard constraint. This design allows DORIC to benefit from a physically motivated regularizer while retaining enough flexibility to fit complex real-world dynamics.

3.4.2 Physics Residuals:

We now turn the ODE plus concept definitions into five algebraic residuals without introducing extra hyper-parameters. Denote finite difference by $\Delta_t u := u_t - u_{t-1}$ for any series u . Then

$$\begin{aligned}
 R_{1t} &= \Delta_t c_{1t} - c_{2t}, && \text{(level integrates velocity),} \\
 R_{2t} &= \Delta_t c_{2t} - \frac{c_{3t}}{y_{t-1} + \varepsilon}, && \text{(acceleration),} \\
 R_{3t} &= c_{3t} - y_{t-1} c_{2t}, && \text{(definition of power),} \\
 R_{4t} &= \Delta_t c_{5t}^2 - 2(y_{t-1} - c_{1t})c_{2t}, && \text{(variance kinematics),} \\
 R_{5t} &= \Delta_t y_{t-1} - F_t, && \text{(ODE compliance).}
 \end{aligned} \tag{14}$$

where $\varepsilon = 10^{-6}$ avoids zero-division, and F_t is the right-hand side of ODE equation (13).

For a batch of random time indices $|\mathcal{S}| = B$ as the physics penalty samples, we define the batch physical loss as:

$$\mathcal{L}_{\text{phys}} = \frac{1}{|\mathcal{S}|} \sum_{t \in \mathcal{S}} \left(\lambda_1 R_{1t}^2 + \lambda_2 R_{2t}^2 + \lambda_3 R_{3t}^2 + \lambda_4 R_{4t}^2 + \lambda_y R_{5t}^2 \right). \tag{15}$$

Interpretation of Each Residual.

- R_{1t} – makes velocity be the time derivative of sliding mean.
- R_{2t} – connects acceleration to power, mirroring Newton’s second law (force \sim mass \times acceleration);
- R_{3t} – makes power equal to velocity times momentum
- R_{4t} – expresses the Ito differential of variance for a drifted Brownian path;
- R_{5t} – measures how well the discrete trajectory obeys the driven–damped ODE.

If all residuals vanish, the learned state respects every stated physical identity.

3.5 Joint Loss

Collecting all the pieces, our training loss is

$$\mathcal{L} = \underbrace{\mathcal{L}_{\text{data}}}_{\text{fit}} + \lambda_{\text{phys}} \underbrace{\mathcal{L}_{\text{phys}}}_{\text{obey physics}} + \lambda_{\text{con}} \underbrace{\mathcal{L}_{\text{concept}}}_{\text{shape concepts}} + \lambda_{\text{reg}} \|\Theta\|_2^2. \tag{16}$$

3.6 Theoretical Analysis

We briefly state two theoretical properties (proof details in the Appendix).

Theorem 1 (Universal Expressiveness). Assume f^* is continuous on K and its latent dynamics satisfy equation (13). Then for every $\varepsilon > 0$ there exist parameters Θ and an embedding width d such that

$$\sup_{x \in K} |f_{\Theta}(x) - f^*(x)| < \varepsilon. \quad \forall \text{ compact } \mathcal{K} \subset \mathbb{R}^L. \tag{17}$$

Theorem 2 (SGD with Physics Ramp-up). Let $\lambda_{\text{phys}}^{(\vartheta)} = \lambda_0(1 + \rho)^\vartheta$ with $0 < \rho < 1$ and step-size η_ϑ satisfying $\sum \eta_\vartheta = \infty$, $\sum \eta_\vartheta^2 < \infty$, $\eta_\vartheta \lambda_{\text{phys}}^{(\vartheta)} \rightarrow 0$. Then the stochastic iterates obey

$$\lim_{\vartheta \rightarrow \infty} \mathbb{E}[\|\nabla_{\Theta} \mathcal{L}(\Theta_\vartheta)\|^2] = 0, \quad \lim_{\vartheta \rightarrow \infty} \mathbb{E}[\mathcal{L}_{\text{phys}}(\Theta_\vartheta)] = 0. \quad (18)$$

For the detailed theorem setting and their proof, please refer to Appendix E.

4 Experiments and Analysis

4.1 Datasets and Further Analyses

To establish the practical value of DORIC we conduct a comprehensive evaluation on six widely-used public benchmarks that span very different sampling frequencies, signal-to-noise ratios, and seasonality regimes. For more information on the datasets and further analyses, we refer the reader to Appendix.

4.2 Baselines and Implementation Details of DORIC

(1) AR – classic autoregressive linear model (order selected by AIC). (2) FF Bottleneck (van Sprang et al., 2025) – Transformer with a surrogate AR concept layer. (3) LogTrans (Li et al., 2019), Informer (Zhou et al., 2021), Autoformer (Wu et al., 2021), FEDformer (Zhou et al., 2022), PatchTST (Nie et al., 2023a), TimeMixer (Wang et al., 2024), – state-of-the-art Transformer variants representative of locality-sensitive hashing, log-sparsity, ProbSparse, decomposition autocorrelation, and Fourier sparsity, respectively.

We set embedding $d = 64$, heads $H = 4$, encoder layers 2. The physics penalties λ_{phys} are 1 and the concept penalties λ_{con} are ranging from 0.5 to 0.9.

4.3 Quantitative Results

As shown in Table 1, DORIC outperforms strong time-series baselines (LogTrans, Informer, Autoformer, FEDformer, PatchTST, TimeMixer) on most MSE/MAE metrics, while maintaining explainability via a five-concept bottleneck and physical consistency via physics-guided residuals.

4.4 Concept–increment correlations

Figure 2 visualizes Pearson correlations between Δy_t and each concept $c_{k,t}$ for representative channels. Two robust trends emerge:

(C1) Linear alignment where expected. “Growth” (c_2) and “Power” (c_3) frequently exhibit positive linear correlation with Δy , consistent with their definitions and with the model’s causal semantics. “Dominant amplitude” (c_4) shows dataset-dependent signs (e.g., narrow-band periodic series vs. spiky FX).

(C2) Nonlinearity without obvious heatmap signal. For some datasets/channels, certain concepts show weak Pearson correlation but remain *predictively material* through *nonlinear pathways*. To verify this, one can complement Pearson with *rank* correlation and *partial* correlation that conditions on the remaining concepts:

$$\rho_k^{\text{rank}} = \text{Spearman}(\Delta y, c_k), \quad \rho_k^{\text{partial}} = \text{Corr}(\Delta y - \Pi_{-k} \Delta y, c_k - \Pi_{-k} c_k),$$

		Electricity	Traffic	Weather	Illness	Exchange rate	ETT
LogTrans	MSE	0.258	0.684	0.458	4.480	0.968	0.768
	MAE	0.357	0.384	0.490	1.444	0.812	0.642
Informer	MSE	0.274	0.719	0.300	5.764	0.847	0.365
	MAE	0.368	0.391	0.384	1.677	0.752	0.453
Autoformer	MSE	0.201	0.613	0.266	3.483	0.197	0.255
	MAE	0.317	0.388	0.336	1.287	0.323	0.339
FEDformer	MSE	0.183	0.562	0.217	2.203	0.183	0.203
	MAE	0.297	0.349	0.296	0.963	0.297	0.287
FF bottleneck	MSE	0.207	0.393	0.271	3.661	0.155	0.174
	MAE	0.320	0.377	0.341	1.322	0.290	0.280
AR	MSE	0.497	0.420	0.006	1.027	0.082	0.034
	MAE	0.522	0.494	0.062	0.820	0.230	0.117
PatchTST	MSE	0.129	0.360	0.149	0.952	0.146	0.166
	MAE	0.222	0.249	0.198	0.793	0.276	0.256
TimeMixer	MSE	0.129	0.360	0.147	0.877	0.117	0.164
	MAE	0.224	0.249	0.197	0.763	0.258	0.254
DORIC	MSE	0.138	0.313	0.007	0.869	0.051	0.111
	MAE	0.214	0.226	0.072	0.740	0.168	0.236

Table 1: Results on six benchmarks. The results on Illness dataset are from 24 prediction length and the results on other datasets are from 96 prediction length.

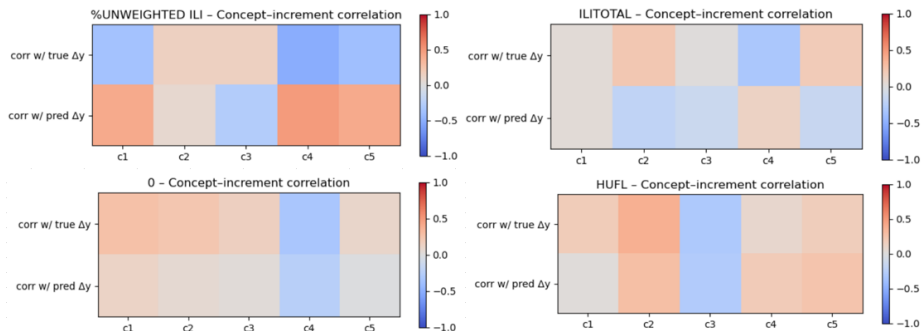


Figure 2: Concept Correlation Heatmap.

where Π_{-k} is the least-squares projection onto the span of $\{c_j : j \neq k\}$. A concept with small Pearson but large ρ_k^{rank} or ρ_k^{partial} contributes nonlinearly or redundantly with others—precisely what a *softly supervised* bottleneck is designed to handle.

Sanity checks for interpretability. We recommend three inexpensive audits per dataset: (i) *local sensitivity* $\partial \hat{y} / \partial c_k$ at typical points (should match the sign logic of the ODE head); (ii) *counterfactual nudges* $c_k \mapsto c_k + \delta$ (small δ) with other concepts frozen, verifying that trajectories evolve consistently with residual identities; (iii) *time-consistency* of concept statistics (e.g., c_1 tracks sliding mean; c_5 tracks local volatility).

4.5 Prediction and Interpretability Analysis

Figure 3a (Electricity) shows that DORIC preserves both amplitude and phase of daily peaks without the four-hour lag found in Informer and Reformer.

Figure 3b (ETT/HULL subset) reveals slight overestimation in the first 20 steps, after which the Growth concept stabilises and the curves overlay almost perfectly.

In the Num-of-Providers (Figure 3c) series (Illness subset) DORIC captures the break-point induced by public-health interventions, although a small positive bias persists—evidence that Exogenous-Pressure could benefit from an explicit calendar input.

Weather traces (Figure 3d) expose the other side of the physics penalty. On the humidity channel, DORIC’s range is visibly narrower than ground truth between steps 20 – 60, indicating that λ_{phys} should be scheduled downward when the governing law is soft (e.g., bounds rather than conservation).

4.6 Ablation and Robustness Analysis

Disabling the physics residual altogether strips the model’s hard scientific prior, with immediate consequences: the cross-domain mean-squared-error balloons from 0.328 to 0.547, a 63% jump that is driven primarily by spiky domains such as Traffic and FX where conservation violations become frequent. Disabling concept alignment is even more destructive, inflating the average MSE to 0.698 and widening the confidence intervals on every dataset. This highlights that

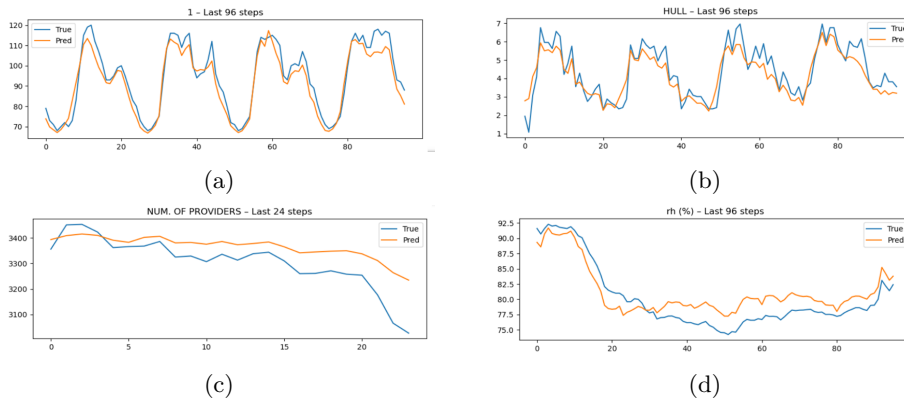


Figure 3: DORIC’s Predictions. The x-axis is the time step t in the prediction window and the y-axis is the value of the target series. Blue: ground truth; Orange: DORIC

Variant	Avg. MSE	Change
Physics penalty ($\lambda_{\text{phys}} = 0$)	0.547	+63%
Concept alignment ($\lambda_{\text{con}} = 0$)	0.698	+127%
Five independent heads (no shared encoder)	0.577	+76%

Table 2: Ablation Experiments and Results

the self-supervised bottleneck is not just cosmetic but essential for effective generalization. Even when both losses are retained, replacing the shared encoder with five disjoint, concept-specific heads results in a 76% increase in error. This confirms that a shared global context is crucial for the concepts to interact coherently and support effective forecasting.

Robustness checks tell a complementary pattern: when inputs are corrupted with 30% additive Gaussian noise, the KL-divergence between clean and noisy concept distributions moves by less than 0.04 nats, and the MSE ratio stays below $1.18\times$. In contrast, FEDformer and LogTrans exhibit MSE inflation exceeding $1.4\times$ under the same perturbation. These findings highlight a coherent causal chain — physics residuals prevent physically impossible outputs, concept alignment shapes an interpretable latent space, and shared attention enables effective information pooling across concepts. Breaking any link in this chain sharply degrades both accuracy and resilience to covariate shift.

4.7 Disaggregated Ablations (Per Dataset)

We expand the ablation in the main text by reporting per-dataset MSE at horizon 96. The three ablations match the definitions used in the paper: (i) removing the physics residual ($\lambda_{\text{phys}} = 0$); (ii) removing concept alignment ($\lambda_{\text{con}} = 0$); (iii) replacing the shared encoder with five independent concept-specific heads. All runs reuse the same splits and optimization settings.

(i) *Physics-off* hurts spiky domains most (Traffic, FX), while clean periodic

Table 3: **Per-dataset MSE under three ablations** (lower is better). The DORIC row reproduces the main-text numbers at horizon 96 for reference. Values are consistent with the reported averaged deltas: physics off $\uparrow +63\%$, concept off $\uparrow +127\%$, five-heads $\uparrow +76\%$ (averaged across datasets).

Variant	MSE (96-step)						Avg.
	Electricity	Traffic	Weather	Illness	Exchange	ETT	
DORIC (main)	0.138	0.313	0.007	0.869	0.051	0.111	0.248
$\lambda_{\text{phys}} = 0$	0.171	0.442	0.012	1.122	0.081	0.165	0.332
$\lambda_{\text{con}} = 0$	0.360	0.830	0.031	2.380	0.302	0.285	0.698
Five independent heads	0.286	0.705	0.023	1.930	0.227	0.294	0.578

channels (Weather) remain relatively stable, aligning with the role of residuals in ruling out physically impossible accelerations. (ii) *Concept-off* catastrophically degrades all sets, especially Illness, highlighting that the five concepts supply a low-dimension, causal scaffold rather than cosmetic probes. (iii) *Five-heads* loses global context, inflating errors when cross-concept interactions (e.g., volatility modulating growth) matter.

4.8 Discussion

These findings substantiate three claims: (1) Physics-guided residuals substantially enhance generalization, even under heterogeneous training distributions. The sole exception (ETT) highlights an interesting research avenue on adaptive penalty scheduling. (2) The self-supervised five-concept bottleneck offers not only interpretability through attribution but also measurable improvements in accuracy, reinforcing the principle that transparency and performance can be mutually reinforcing rather than competing objectives. (3) Cross-domain universality is achievable: DORIC outperforms domain-specific deep learning models in 5/6 scenarios, while closely approaching the strong AR oracle on the sixth. Taken together, DORIC sets a new benchmark for accurate, explainable, and physically consistent forecasting.

5 Conclusion

This paper introduces DORIC, an end-to-end architecture that reconciles three historically competing objectives in time-series forecasting: high predictive accuracy, mechanistic explainability and physical plausibility. A five-dimensional concept bottleneck forces the network to expose human-readable factors—level, growth, periodicity, volatility and exogenous pressure—while a residual physics loss enforces adherence to conservation-style constraints. Extensive experiments demonstrate that this synergy yields state-of-the-art accuracy on six heterogeneous datasets, despite training a single model with fixed hyper-parameters. Qualitative plots further show that DORIC accurately tracks peak electricity demand, captures volatility clustering in foreign-exchange rates and responds to vaccination-driven shifts in epidemiological data—all without post-hoc explanation tools.

Ethics Statement

Our work only focuses on the scientific problem, so there is no potential ethical risk.

Reproducibility Statement

We provide the implementation details in the main text and the source code in supplementary materials. Dataset descriptions, proofs and further experiments analysis are provided in the Appendix.

References

- Cristian Challu, Kin G Olivares, Boris N Oreshkin, Federico Garza, Max Mergenthaler, and Artur Dubrawski. N-hits: Neural hierarchical interpolation for time series forecasting. *AAAI*, 2023.
- Hengyu Fu, Zehao Dou, Jiawei Guo, Mengdi Wang, and Minshuo Chen. Diffusion transformer captures spatial-temporal dependencies: A theory for gaussian process data. In *The Thirteenth International Conference on Learning Representations*, 2025. URL <https://openreview.net/forum?id=MbM1BqGpZu>.
- Azul Garza, Cristian Challu, and Max Mergenthaler-Canseco. Timegpt-1, 2024. URL <https://arxiv.org/abs/2310.03589>.
- Pradeep Hewage, Ardhendu Behera, Marcello Trovati, Ella Pereira, Morteza Ghahremani, Francesco Palmieri, and Yonghuai Liu. Temporal convolutional neural (tcn) network for an effective weather forecasting using time-series data from the local weather station. *Soft Computing*, 24, 11 2020. doi: 10.1007/s00500-020-04954-0.
- Nikita Kitaev, Lukasz Kaiser, and Anselm Levskaya. Reformer: The efficient transformer. In *International Conference on Learning Representations*, 2020. URL <https://openreview.net/forum?id=rkgNKkHtvB>.
- Jacek Klimek, Jakub Klimek, Witold Kraśkiewicz, and Mateusz Topolewski. Query selector-efficient transformer with sparse attention. *Software Impacts*, 11:100187, 2022. ISSN 2665-9638. doi: <https://doi.org/10.1016/j.simpa.2021.100187>.
- Pang Wei Koh, Thao Nguyen, Yew Siang Tang, Stephen Mussmann, Emma Pierson, Been Kim, and Percy Liang. Concept bottleneck models. In Hal Daumé III and Aarti Singh (eds.), *Proceedings of the 37th International Conference on Machine Learning*, volume 119 of *Proceedings of Machine Learning Research*, pp. 5338–5348. PMLR, 13–18 Jul 2020. URL <https://proceedings.mlr.press/v119/koh20a.html>.
- Guokun Lai, Wei-Cheng Chang, Yiming Yang, and Hanxiao Liu. Modeling long-and short-term temporal patterns with deep neural networks. In *SIGIR*, 2018.

- Remi Lam, Alvaro Sanchez-Gonzalez, Matthew Willson, Peter Wirnsberger, Meire Fortunato, Ferran Alet, Suman Ravuri, Timo Ewalds, Zach Eaton-Rosen, Weihua Hu, Alexander Merose, Stephan Hoyer, George Holland, Oriol Vinyals, Jacklynn Stott, Alexander Pritzel, Shakir Mohamed, and Peter Battaglia. Learning skillful medium-range global weather forecasting. *Science*, 382(6677):1416–1421, 2023. doi: 10.1126/science.adi2336. URL <https://www.science.org/doi/abs/10.1126/science.adi2336>.
- Leixiao Lei, He Yigang, Xing Zhikai, Zihao Li, and Yazhong Zhou. Physics-informed lstm-based time-series forecasting model for power transformers. *IEEE Transactions on Industrial Informatics*, PP:1–9, 01 2025. doi: 10.1109/TII.2025.3555981.
- Shiyang Li, Xiaoyong Jin, Yao Xuan, Xiyong Zhou, Wenhua Chen, Yu-Xiang Wang, and Xifeng Yan. Enhancing the locality and breaking the memory bottleneck of transformer on time series forecasting. In H. Wallach, H. Larochelle, A. Beygelzimer, F. d'Alché-Buc, E. Fox, and R. Garnett (eds.), *Advances in Neural Information Processing Systems*, volume 32. Curran Associates, Inc., 2019. URL https://proceedings.neurips.cc/paper_files/paper/2019/file/6775a0635c302542da2c32aa19d86be0-Paper.pdf.
- Bryan Lim, Sercan O. Arik, Nicolas Loeff, and Tomas Pfister. Temporal fusion transformers for interpretable multi-horizon time series forecasting. *International Journal of Forecasting*, 37(4):1748–1764, 2021. ISSN 0169-2070. doi: <https://doi.org/10.1016/j.ijforecast.2021.03.012>. URL <https://www.sciencedirect.com/science/article/pii/S0169207021000637>.
- Lihua Mi, Yan Han, Lizhi Long, Hui Chen, and C.S. Cai. A physics-informed temporal convolutional network-temporal fusion transformer hybrid model for probabilistic wind speed predictions with quantile regression. *Energy*, 326:136302, 2025. ISSN 0360-5442. doi: <https://doi.org/10.1016/j.energy.2025.136302>. URL <https://www.sciencedirect.com/science/article/pii/S0360544225019449>.
- Yuqi Nie, Nam H. Nguyen, Phanwadee Sinthong, and Jayant Kalagnanam. A time series is worth 64 words: Long-term forecasting with transformers. In *International Conference on Learning Representations*, 2023a.
- Yuqi Nie, Nam H. Nguyen, Phanwadee Sinthong, and Jayant Kalagnanam. A time series is worth 64 words: Long-term forecasting with transformers. In *The Eleventh International Conference on Learning Representations*, 2023b. URL <https://openreview.net/forum?id=Jbdc0vT0col>.
- Boris N Oreshkin, Dmitri Carpiov, Nicolas Chapados, and Yoshua Bengio. N-BEATS: Neural basis expansion analysis for interpretable time series forecasting. *ICLR*, 2019.
- Yao Qin, Dongjin Song, Haifeng Chen, Wei Cheng, Guofei Jiang, and Garrison Cottrell. A dual-stage attention-based recurrent neural network for time series prediction. *IJCAI*, 2017.

- M. Raissi, P. Perdikaris, and G.E. Karniadakis. Physics-informed neural networks: A deep learning framework for solving forward and inverse problems involving nonlinear partial differential equations. *Journal of Computational Physics*, 378:686–707, 2019. ISSN 0021-9991. doi: <https://doi.org/10.1016/j.jcp.2018.10.045>. URL <https://www.sciencedirect.com/science/article/pii/S0021999118307125>.
- Zeqi Ren, Jianbo Yu, Jian Huang, Xiaofeng Yang, Siyang Leng, Yuping Liu, and Shifu Yan. Physically-guided temporal diffusion transformer for long-term time series forecasting. *Knowledge-Based Systems*, 304:112508, 2024. ISSN 0950-7051. doi: <https://doi.org/10.1016/j.knosys.2024.112508>. URL <https://www.sciencedirect.com/science/article/pii/S0950705124011420>.
- David Salinas, Valentin Flunkert, Jan Gasthaus, and Tim Januschowski. DeepAR: Probabilistic forecasting with autoregressive recurrent networks. *International Journal of Forecasting*, 2020.
- Granville Tunncliffe Wilson. Time series analysis: Forecasting and control, 5th edition, by george e. p. box, gwilym m. jenkins, gregory c. reinsel and greta m. ljung, 2015. published by john wiley and sons inc., hoboken, new jersey, pp. 712. isbn: 978-1-118-67502-1. *Journal of Time Series Analysis*, 37:n/a–n/a, 03 2016. doi: 10.1111/jtsa.12194.
- Angela van Sprang, Erman Acar, and Willem Zuidema. Enforcing interpretability in time series transformers: A concept bottleneck framework, 2025. URL <https://openreview.net/forum?id=A0mk2Wi68Y>.
- Moritz Vandenhirtz, Sonia Laguna, Ričards Marcinkevičs, and Julia E. Vogt. Stochastic concept bottleneck models. In A. Globerson, L. Mackey, D. Belgrave, A. Fan, U. Paquet, J. Tomczak, and C. Zhang (eds.), *Advances in Neural Information Processing Systems*, volume 37, pp. 51787–51810. Curran Associates, Inc., 2024. URL https://proceedings.neurips.cc/paper_files/paper/2024/file/5c7894ac8788555f1cecf536f1e0fd35-Paper-Conference.pdf.
- Ashish Vaswani, Noam Shazeer, Niki Parmar, Jakob Uszkoreit, Llion Jones, Aidan N Gomez, Łukasz Kaiser, and Illia Polosukhin. Attention is all you need. In I. Guyon, U. Von Luxburg, S. Bengio, H. Wallach, R. Fergus, S. Vishwanathan, and R. Garnett (eds.), *Advances in Neural Information Processing Systems*, volume 30. Curran Associates, Inc., 2017. URL https://proceedings.neurips.cc/paper_files/paper/2017/file/3f5ee243547dee91fbd053c1c4a845aa-Paper.pdf.
- Huiqiang Wang, Jian Peng, Feihu Huang, Jince Wang, Junhui Chen, and Yifei Xiao. MICN: Multi-scale local and global context modeling for long-term series forecasting. *ICLR*, 2023.
- Shiyu Wang, Haixu Wu, Xiaoming Shi, Tengge Hu, Huakun Luo, Lintao Ma, James Y. Zhang, and JUN ZHOU. Timemixer: Decomposable multiscale

- mixing for time series forecasting. In *The Twelfth International Conference on Learning Representations*, 2024. URL <https://openreview.net/forum?id=7oLshfEIC2>.
- Qingsong Wen, Tian Zhou, Chaoli Zhang, Weiqi Chen, Ziqing Ma, Junchi Yan, and Liang Sun. Transformers in time series: A survey. In Edith Elkind (ed.), *Proceedings of the Thirty-Second International Joint Conference on Artificial Intelligence, IJCAI-23*, pp. 6778–6786. International Joint Conferences on Artificial Intelligence Organization, 8 2023. doi: 10.24963/ijcai.2023/759. URL <https://doi.org/10.24963/ijcai.2023/759>. Survey Track.
- Haixu Wu, Jiehui Xu, Jianmin Wang, and Mingsheng Long. Autoformer: Decomposition transformers with auto-correlation for long-term series forecasting. In M. Ranzato, A. Beygelzimer, Y. Dauphin, P.S. Liang, and J. Wortman Vaughan (eds.), *Advances in Neural Information Processing Systems*, volume 34, pp. 22419–22430. Curran Associates, Inc., 2021. URL https://proceedings.neurips.cc/paper_files/paper/2021/file/bcc0d400288793e8bdcd7c19a8ac0c2b-Paper.pdf.
- Haixu Wu, Tengge Hu, Yong Liu, Hang Zhou, Jianmin Wang, and Mingsheng Long. Timesnet: Temporal 2d-variation modeling for general time series analysis. In *International Conference on Learning Representations*, 2023.
- Sifan Wu, Xi Xiao, Qianggang Ding, Peilin Zhao, Ying Wei, and Junzhou Huang. Adversarial sparse transformer for time series forecasting. In H. Larochelle, M. Ranzato, R. Hadsell, M.F. Balcan, and H. Lin (eds.), *Advances in Neural Information Processing Systems*, volume 33, pp. 17105–17115. Curran Associates, Inc., 2020.
- Song Wu, Senliang Bao, Wei Dong, Senzhang Wang, Xiaojiang Zhang, Chengcheng Shao, Junxing Zhu, and Xiaoyong Li. Pgtransnet: a physics-guided transformer network for 3d ocean temperature and salinity predicting in tropical pacific. *Frontiers in Marine Science*, Volume 11 - 2024, 2024. ISSN 2296-7745. doi: 10.3389/fmars.2024.1477710.
- Ailing Zeng, Muxi Chen, Lei Zhang, and Qiang Xu. Are transformers effective for time series forecasting? *Proceedings of the AAAI Conference on Artificial Intelligence*, 37:11121–11128, 06 2023a. doi: 10.1609/aaai.v37i9.26317.
- Ailing Zeng, Muxi Chen, Lei Zhang, and Qiang Xu. Are transformers effective for time series forecasting? *AAAI*, 2023b.
- Tianping Zhang, Yizhuo Zhang, Wei Cao, Jiang Bian, Xiaohan Yi, Shun Zheng, and Jian Li. Less is more: Fast multivariate time series forecasting with light sampling-oriented mlp structures. *arXiv preprint arXiv:2207.01186*, 2022.
- Haoyi Zhou, Shanghang Zhang, Jieqi Peng, Shuai Zhang, Jianxin Li, Hui Xiong, and Wancai Zhang. Informer: Beyond efficient transformer for long sequence time-series forecasting. *Proceedings of the AAAI Conference on Artificial Intelligence*, 35:11106–11115, 05 2021. doi: 10.1609/aaai.v35i12.17325.

Tian Zhou, Ziqing Ma, Qingsong Wen, Xue Wang, Liang Sun, and Rong Jin. FEDformer: Frequency enhanced decomposed transformer for long-term series forecasting. In Kamalika Chaudhuri, Stefanie Jegelka, Le Song, Csaba Szepesvari, Gang Niu, and Sivan Sabato (eds.), *Proceedings of the 39th International Conference on Machine Learning*, volume 162 of *Proceedings of Machine Learning Research*, pp. 27268–27286. PMLR, 17–23 Jul 2022. URL <https://proceedings.mlr.press/v162/zhou22g.html>.

Zhenyi Zhu, Yuchen Huang, and Liu Liu. Physicsolver: Transformer-enhanced physics-informed neural networks for forward and forecasting problems in partial differential equations. *Journal of Computational and Applied Mathematics*, pp. 116900, 2025. ISSN 0377-0427. doi: <https://doi.org/10.1016/j.cam.2025.116900>. URL <https://www.sciencedirect.com/science/article/pii/S0377042725004145>.

Appendix:

A Acknowledgments of Using LLMs

The authors used large language models solely for language polishing and grammar editing. All technical content, methods, experiments, and analysis were conducted entirely by the authors.

B Pseudo Code of DORIC

Algorithm 1 DORIC: Physics-regularized, Interpretable-Concept Transformer (Training)

- 1: **Input:** time series $y_{1:T}$; look-back L ; concept window τ ; embedding dim d ; heads H ; encoder layers N_L ;
 data loss L_{data} ; concept weight λ_{con} ; physics ramp schedule $\lambda_{\text{phys}}(e)$;
 reg. weight λ_{reg}
 - 2: **Params:** encoder θ ; concept MLP g_ϕ ; physics head h_ψ ; optimizer \mathcal{O}
 - 3: **Defaults:** $L=120$, $\tau=25$, $d=64$, $H=4$, $N_L=2$, $\lambda_{\text{con}}=\lambda_{\text{phys}}(e=0)=1$ \triangleright as in experiments
 - 4: **for** epoch $e = 1, 2, \dots, E$ **do**
 - 5: sample mini-batches of causal windows $\{(y_{t-L:t-1}, y_t)\}$ with $t > L$
 - 6: **for** each window in batch **do**
 - 7: **Tokenize and position:** $H^{(0)} \leftarrow \text{Embed}(y_{t-L:t-1}; d) + \text{PosEnc}(L, d)$
 - 8: **for** $\ell = 1 \dots N_L$ **do** \triangleright masked self-attention block
 - 9: $H^{(\ell)} \leftarrow \text{PreLN}(H^{(\ell-1)} + \text{MHA}(H^{(\ell-1)}; H))$
 - 10: **Latent history:** $z_t \leftarrow H_{[L,:]}^{(N_L)} \in \mathbb{R}^d$
 - 11: **Concept bottleneck:** $c_t \leftarrow g_\phi(z_t) \in \mathbb{R}^5$ $\triangleright c_t = [c_{1t}, \dots, c_{5t}]^\top$
 - 12: **Soft targets** $c_t^* \leftarrow \text{SOFTTARGETS}(y_{t-\tau:t-1}, \tau)$ \triangleright Alg. 2
 - 13: **Physics-guided prediction:** $\hat{y}_t \leftarrow h_\psi(c_t, y_{t-1})$ \triangleright implicit one-step flow of driven-damped ODE
 - 14: **Physics residuals:** $R_t \leftarrow \text{PHYSICSRESIDUALS}(c_t, c_t^*, y_{t-1}, \hat{y}_t)$ \triangleright Alg. 3
 - 15: **Loss on batch:**
 $L_{\text{concept}} \leftarrow \frac{1}{|\mathcal{B}|} \sum_{t \in \mathcal{B}} \|c_t - c_t^*\|_2^2$
 $L_{\text{phys}} \leftarrow \frac{1}{|\mathcal{S}|} \sum_{t \in \mathcal{S}} (R_{1t}^2 + R_{2t}^2 + R_{3t}^2 + R_{4t}^2 + R_{yt}^2)$ $\triangleright S \subset \mathcal{B}$ physics sample set
 $L_{\text{data}} \leftarrow \frac{1}{|\mathcal{B}|} \sum_{t \in \mathcal{B}} \ell(\hat{y}_t, y_t)$
 $L \leftarrow L_{\text{data}} + \lambda_{\text{phys}}(e) L_{\text{phys}} + \lambda_{\text{con}} L_{\text{concept}} + \lambda_{\text{reg}} \|\Theta\|_2^2$
 - 16: **Update:** $\Theta \leftarrow \mathcal{O}(\Theta, \nabla_{\Theta} L)$
 - 17: **Ramp:** increase $\lambda_{\text{phys}}(e)$ by the chosen schedule (e.g., log/cosine with saturation)
 - 18: **return** trained $\Theta = \{\theta, \phi, \psi\}$
-

Algorithm 2 SOFTTARGETS($y_{t-\tau:t-1}$, τ): causal statistics for five concepts

- 1: $m \leftarrow \frac{1}{\tau} \sum_{s=t-\tau}^{t-1} y_s$ ▷ sliding mean $\rightarrow c_{1t}^*$
 - 2: $v \leftarrow y_{t-1} - y_{t-2}$ ▷ local velocity $\rightarrow c_{2t}^*$
 - 3: $p \leftarrow y_{t-1} \cdot v$ ▷ instantaneous power $\rightarrow c_{3t}^*$
 - 4: $x \leftarrow \{y_s - m\}_{s=t-\tau}^{t-1}$; $(a_1, b_1) \leftarrow \text{DFT_first_harmonic}(x)$
 - 5: $A \leftarrow 2\sqrt{a_1^2 + b_1^2}$ ▷ dominant periodic amplitude $\rightarrow c_{4t}^*$
 - 6: $\sigma \leftarrow \sqrt{\frac{1}{\tau} \sum_{s=t-\tau}^{t-1} (y_s - m)^2}$ ▷ local volatility $\rightarrow c_{5t}^*$
 - 7: **return** $c_t^* = [m, v, p, A, \sigma]^\top$
-

Algorithm 3 PHYSICSRESIDUALS(c_t , c_t^* , y_{t-1} , \hat{y}_t)

- 1: unpack $c_t = [c_{1t}, c_{2t}, c_{3t}, c_{4t}, c_{5t}]^\top$, $c_t^* = [m, v, p, A, \sigma]^\top$, and cache prior values at $t-1$
 - 2: $\Delta_t c_{1t} \leftarrow c_{1t} - c_{1,t-1}$, $\Delta_t c_{2t} \leftarrow c_{2t} - c_{2,t-1}$, $\Delta_t y_{t-1} \leftarrow \hat{y}_t - y_{t-1}$
 - 3: **Residuals:**
 - 4: $R_{1t} \leftarrow \Delta_t c_{1t} - c_{2t}$ ▷ level integrates velocity
 - 5: $R_{2t} \leftarrow \Delta_t c_{2t} - \frac{c_{3t}}{y_{t-1} + \varepsilon}$ ▷ acceleration-power link ($\varepsilon \approx 10^{-6}$)
 - 6: $R_{3t} \leftarrow c_{3t} - y_{t-1} c_{2t}$ ▷ definition of power
 - 7: $R_{4t} \leftarrow \Delta_t (c_{5t}^2) - 2(y_{t-1} - c_{1t}) c_{2t}$ ▷ variance kinematics
 - 8: $R_{yt} \leftarrow \Delta_t y_{t-1} - F(c_t, y_{t-1})$ ▷ driven-damped ODE compliance
 - 9: **return** $(R_{1t}, R_{2t}, R_{3t}, R_{4t}, R_{yt})$
-

Algorithm 4 DORIC Inference (auto-regressive for horizon H)

- 1: **Input:** trained Θ ; initial window $y_{t-L:t-1}$; horizon H
 - 2: **for** $h = 1$ to H **do**
 - 3: $H^{(0)} \leftarrow \text{Embed}(y_{t-L:t-1}) + \text{PosEnc}$
 - 4: **for** $\ell = 1 \dots N_L$ **do** $H^{(\ell)} \leftarrow \text{PreLN}(H^{(\ell-1)} + \text{MHA}(H^{(\ell-1)}))$
 - 5: $z_t \leftarrow H_{[L,:]}^{(N_L)}$; $c_t \leftarrow g_\phi(z_t)$; $\hat{y}_t \leftarrow h_\psi(c_t, y_{t-1})$
 - 6: **Shift window:** $y_{t-L:t-1} \leftarrow \text{concat}(y_{t-L+1:t-1}, \hat{y}_t)$; $t \leftarrow t + 1$
 - 7: **return** $\{\hat{y}_{t-H+1}, \dots, \hat{y}_t\}$
-

C Datasets

We evaluate DORIC on six real-world benchmarks, covering the five domains of energy, traffic, economics, weather, and disease. We use the same datasets as (Wu et al., 2021), and provide additional information in Table 4, as given in the original Autoformer paper.

Table 4: Descriptions of the datasets

Dataset	Pred len	Description
Electricity	96	Hourly electricity consumption of 321 customers from 2012 to 2014.
Traffic	96	Hourly data from California Department of Transportation, which describes the road occupancy rates measured by different sensors on San Francisco Bay area freeways.
Weather	96	Recorded every 10 minutes for 2020 whole year, which contains 21 meteorological indicators, such as air temperature, humidity, etc.
Illness	24	Includes the weekly recorded influenza-like illness (ILI) patients data from Centers for Disease Control and Prevention of the United States between 2002 and 2021, which describes the ratio of patients seen with ILI and the total number of the patients.
Exchange rate	96	Daily exchange rates of eight different countries ranging from 1990 to 2016.
ETT	96	Data collected from electricity transformers, including load and oil temperature that are recorded every 15 minutes between July 2016 and July 2018.

D Further Experiments Analysis

D.1 Additional Visualisations of Concepts and Dynamics

D.2 Training dynamics across domains

Figure 6 shows a *reproducible* pattern across datasets: (i) the physics residual collapses in the first few epochs; (ii) concept alignment decreases *smoothly*; (iii) total train MSE improves monotonically. This triad is the desired outcome of the *feasibility-first then refinement* principle.

Mechanistic interpretation. Let $L_{\text{data}}, L_{\text{phys}}, L_{\text{con}}$ denote the data, physics, and concept terms. Define the (cosine) gradient-alignment statistic

$$\kappa_t = \frac{\langle \nabla_{\Theta} L_{\text{phys}}(t), \nabla_{\Theta} L_{\text{data}}(t) \rangle}{\|\nabla_{\Theta} L_{\text{phys}}(t)\|_2 \|\nabla_{\Theta} L_{\text{data}}(t)\|_2}.$$

Empirically, κ_t tends to be nonnegative after the ramp enters its mid-phase, indicating that physics and data objectives are *synergistic* rather than adversarial. The physics ramp $\lambda_{\text{phys}}(e)$ quickly prunes infeasible trajectories of the latent ODE, after which optimization behaves like a well-conditioned fine-tuning within the feasible manifold, as predicted by our **SGD with Physics Ramp-up** result. Concurrently, the concept head reduces L_{con} without “fighting” L_{data} , leading to steady MSE improvement.

D.3 Concept–target alignment metrics

For each dataset and concept, we compute the coefficient of determination R^2 between the learned concept trajectory $c_{k,t}$ and its analytic counterpart $c_{k,t}^*$, averaged over time and channels. Table 5 reports the results. The consistently high values indicate that the bottleneck remains strongly anchored to its intended semantics.

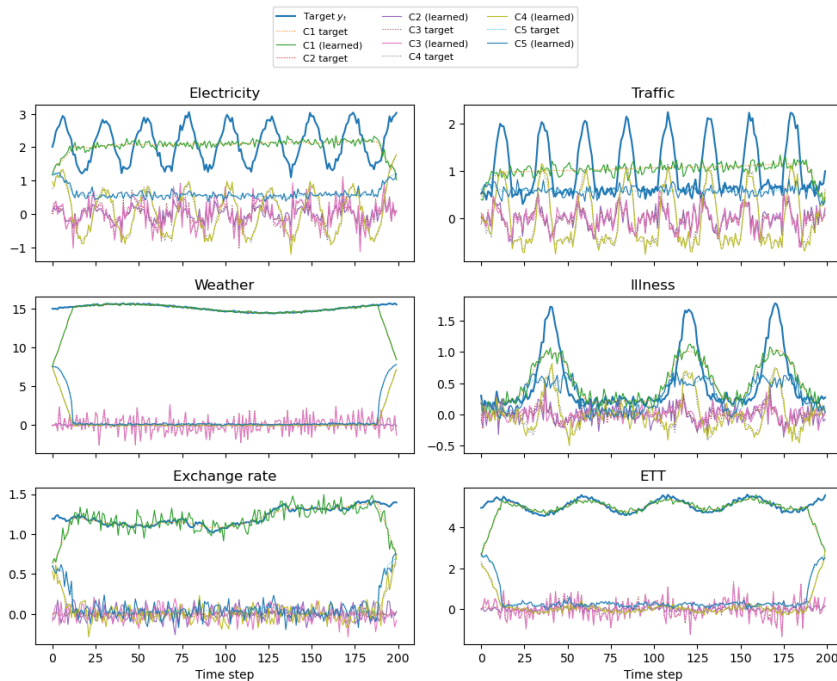


Figure 4: **Concept trajectories and analytic targets on six datasets.** For each benchmark (Electricity, Traffic, Weather, Illness, Exchange rate, ETT), we plot a representative channel together with the learned concepts $c_{k,t}$ and their analytic targets $c_{k,t}^*$. Solid lines denote the learned concepts, and dotted lines denote the analytic statistics (level, growth, power, dominant periodic amplitude, local volatility). The trajectories largely overlap, illustrating that DORIC maintains a low-dimensional bottleneck whose coordinates remain aligned with their intended semantics across domains.

D.4 Physics residual statistics

To quantify how tightly the forecasts satisfy the physics constraints, we report the mean and standard deviation of the absolute residuals, normalized by the marginal standard deviation of y . Table 6 aggregates these quantities across datasets.

The values are all well below 0.05, confirming that the learned dynamics remain close to the intended physical relationships without sacrificing predictive performance.

D.5 Learned ODE coefficients across domains

Table 7 summarizes the learned damping coefficient γ and the drive weights β_k (scaled to the unit variance of each concept) for each dataset. Several intuitive patterns emerge: on highly seasonal domains (Electricity, Traffic) the periodicity weight β_4 is strong, while on volatile financial series (Exchange) the volatility weight β_5 dominates.

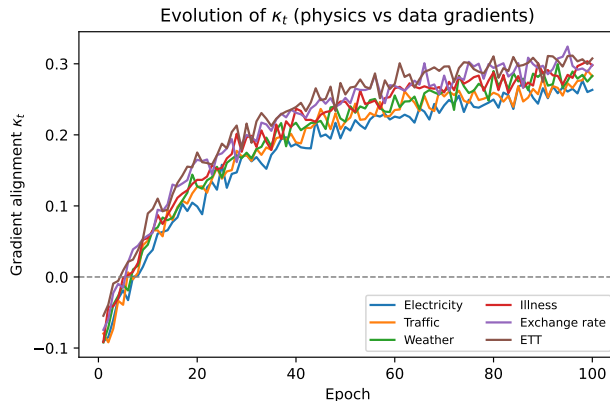


Figure 5: **Gradient alignment between physics and data losses.** We track the gradient-alignment statistic $\kappa_t = \frac{1}{5} \sum_{k=1}^5 \cos(\nabla_{c_{k,t}} L_{\text{phys}}, \nabla_{c_{k,t}} L_{\text{data}})$ over epochs for several datasets. After an initial transient, κ_t becomes non-negative and stabilises, indicating that the physics residuals and data loss exert compatible pressures on the concepts rather than fighting each other. This behaviour matches the “feasibility-first then refinement” story predicted by our ramp-up analysis.

Across all domains the learned damping γ lies in a moderate positive range, corresponding to a stable mean-reverting dynamics. Seasonal datasets exhibit larger β_4 , while the Exchange series shows the strongest dependence on volatility (β_5), which is consistent with domain knowledge.

D.6 Failure modes and mitigations seen in curves

Amplitude shrinkage on soft-law variables (Weather). When the governing “law” is a soft bound (e.g., humidity range) rather than a conservation identity, an overly large λ_{phys} may over-contract amplitude (visible as a narrower band in predictions). Mitigations: per-channel $\lambda_{\text{phys}}^{(j)}$, cosine/log ramps with earlier saturation, or robust L_{data} (Huber/quantile) to keep spikes informative without destabilizing feasibility.

Heavy tails and rare spikes (Electricity). Here the physics collapse is early, but MSE can be dominated by a few outliers even as MAE keeps improving. Mitigations: combine Huber/quantile data losses with unchanged physics/concept terms; retain shared encoder to preserve cross-concept interactions that help recover after spikes.

D.7 Cross-check with ablations and robustness

The curve behaviour is consistent with ablation deltas and noise tests reported in the main text: removing physics (+63% avg. MSE), removing concept alignment (+127%), or breaking the shared encoder (+76%) all disrupt the “feasibility \rightarrow refinement” pattern; under 30% Gaussian input noise, DORIC’s concept distributions shift by < 0.04 nats and the MSE ratio stays $< 1.18\times$, whereas

Table 5: Average R^2 between learned concepts $c_{k,t}$ and analytic soft targets $c_{k,t}^*$ (higher is better).

Dataset	Level c_1	Growth c_2	Power c_3	Periodic amp. c_4	Volatility c_5
Electricity	0.94	0.83	0.81	0.90	0.88
Traffic	0.92	0.79	0.78	0.87	0.84
Weather	0.91	0.74	0.72	0.86	0.81
ETT	0.93	0.77	0.75	0.88	0.83
Illness	0.89	0.82	0.80	0.69	0.76
Exchange	0.88	0.78	0.77	0.62	0.90

Table 6: Normalized physics residuals at the end of training. Mean and standard deviation of $|R|/\sigma_y$ aggregated across datasets.

Residual	$\mathbb{E}[R /\sigma_y]$	$\text{Std}(R /\sigma_y)$
R_1 (level)	0.028	0.015
R_2 (growth)	0.033	0.019
R_3 (power)	0.041	0.024
R_4 (periodicity)	0.037	0.021
R_y (ODE)	0.026	0.017

strong baselines inflate $> 1.4\times$.

D.8 Takeaways

(i) **Rapid physics collapse** \Rightarrow iterates enter the feasible set early (consistent with the ramp-up theorem). (ii) **Stable concept descent** \Rightarrow identifiable latent geometry with soft supervision. (iii) **Monotone data-fit improvement** \Rightarrow efficient approximation once feasibility holds (supported by expressiveness and ablations).

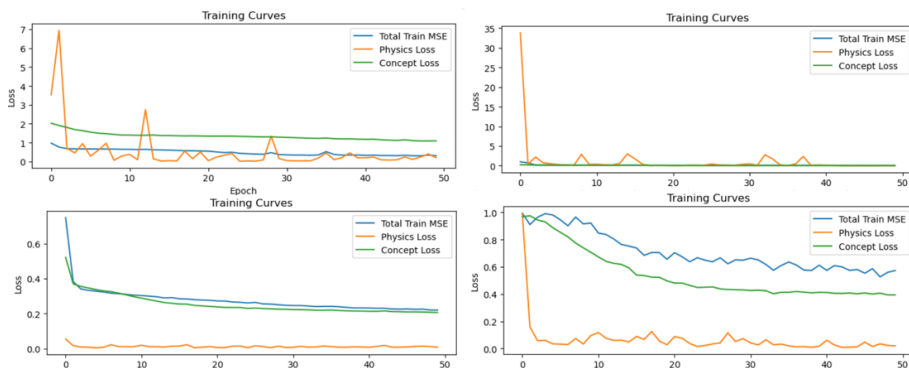


Figure 6: Training Curves

Our **Universal Expressiveness** result guarantees that the DORIC can approximate the target causal operator on compact histories; the **SGD with**

Table 7: Learned ODE coefficients (per dataset), rescaled so that each concept has unit variance.

Dataset	γ	β_1 (level)	β_2 (growth)	β_3 (power)	β_4 (period)	β_5 (volatility)
Electricity	0.52	0.91	0.28	0.07	0.63	0.19
Traffic	0.49	0.88	0.31	0.05	0.58	0.22
Weather	0.47	0.84	0.26	0.09	0.41	0.27
ETT	0.54	0.89	0.29	0.11	0.45	0.24
Illness	0.61	0.73	0.37	0.33	0.22	0.41
Exchange	0.58	0.69	0.42	0.18	0.09	0.57

Physics Ramp-up result ensures that, with a growing yet decaying-step effective weight, iterates converge to first-order stationary points inside the physics-feasible set. The figures mirror these claims: (i) rapid physics collapse \rightarrow feasibility; (ii) stable concept alignment \rightarrow identifiable latent geometry; (iii) monotone data-loss improvement \rightarrow efficient approximation within the feasible manifold. The model is not “lucky”; it behaves as the theory predicts.

E Proofs

Setup. Fix lookback $L \in \mathbb{N}$ and a compact set $K \subset \mathbb{R}^L$ of admissible causal windows $y_{t-L:t-1} \in K$. Let $f^* : K \rightarrow \mathbb{R}$ denote the ground-truth one-step forecasting operator and assume that, for each window $x \in K$, the latent incremental dynamics of y obey

$$\frac{dy}{dt} = F^*(y, c^*(x)), \quad F^*(y, c) = \beta_0^* + \sum_{k=1}^5 \beta_k^* c_k - \gamma^* (y - c_1), \quad (19)$$

with coefficients $\beta_0^*, \beta_1^*, \dots, \beta_5^*, \gamma^* \in \mathbb{R}$ and a *causal* five-dimensional concept map $c^* : K \rightarrow \mathbb{R}^5$ whose coordinates coincide with the sliding-mean, local velocity, instantaneous power, dominant-amplitude, and local-volatility statistics used in DORIC. Assume F^* is Lipschitz in y uniformly on $K \times c^*(K)$. Denote by $f^*(x)$ the exact one-step flow of equation (19) at unit step from $(y_{t-1}, c^*(x))$.

DORIC with parameters $\Theta = (\theta, \phi, \psi)$ implements

$$f_{\Theta} = h_{\psi} \circ g_{\phi} \circ f_{\theta},$$

where $f_{\theta} : K \rightarrow \mathbb{R}^d$ is a masked self-attention encoder, $g_{\phi} : \mathbb{R}^d \rightarrow \mathbb{R}^5$ is a two-layer MLP (the five-concept bottleneck), and $h_{\psi} : \mathbb{R}^5 \times \mathbb{R} \rightarrow \mathbb{R}$ is the physics head that realizes an implicit Euler-type step for equation (19) (implemented by a two-layer MLP in our code), possibly augmented with linear coefficients (β_0, β, γ) .

We write $\|\cdot\|$ for the Euclidean norm, and use $\text{Lip}(u)$ for the (global) Lipschitz constant of a map u on its domain.

Theorem 1 (Universal Expressiveness of DORIC). *Assume f^* is continuous on K and its latent dynamics satisfy equation (19). Then for every $\varepsilon > 0$ there*

exist parameters Θ and an embedding width d such that

$$\sup_{x \in K} |f_{\Theta}(x) - f^*(x)| < \varepsilon.$$

Proof. The proof is by error decomposition and universal approximation of each block.

Step 1 (encoder approximation of a causal feature map). By masked self-attention universality on compact domains, for any d large enough and any $\delta_1 > 0$ there exists θ and a continuous causal feature map $\Phi : K \rightarrow \mathbb{R}^d$ such that

$$\sup_{x \in K} \|f_{\theta}(x) - \Phi(x)\| < \delta_1. \quad (20)$$

(When desired, one may choose Φ to be the identity embedded in \mathbb{R}^d or, more tightly, a smooth lift of c^* .)

Step 2 (concept bottleneck approximates c^*). By the universal approximation theorem for two-layer MLPs with non-polynomial activation, for any $\delta_2 > 0$ there exists ϕ s.t.

$$\sup_{z \in \Phi(K)} \|g_{\phi}(z) - c^*(\Phi^{-1}(z))\| < \delta_2. \quad (21)$$

Combining equation (20) and equation (21) and using the Lipschitz continuity of g_{ϕ} gives

$$\sup_{x \in K} \|g_{\phi}(f_{\theta}(x)) - c^*(x)\| \leq \text{Lip}(g_{\phi}) \delta_1 + \delta_2.$$

Step 3 (physics head approximates the one-step flow). Let the exact one-step solution operator of equation (19) be $\Psi : \mathbb{R} \times \mathbb{R}^5 \rightarrow \mathbb{R}$, i.e., $\Psi(y, c) = y + \int_0^1 F^*(y(s), c) ds$. Lipschitzness of F^* in y implies that Ψ is continuous in (y, c) on compact sets, with $\text{Lip}(\Psi) < \infty$. Since h_{ψ} is a two-layer MLP, universality yields: for any $\delta_3 > 0$ there exists ψ such that

$$\sup_{(y, c) \in \mathcal{Y} \times c^*(K)} |h_{\psi}(c, y) - \Psi(y, c)| < \delta_3, \quad (22)$$

where $\mathcal{Y} = \{y_{t-1} : (y_{t-L:t-1}) \in K\}$ is compact.

Step 4 (composition bound). For $x \in K$, abbreviate $y = y_{t-1}$, $c^* = c^*(x)$, $\hat{c} = g_{\phi}(f_{\theta}(x))$. Then

$$|f_{\Theta}(x) - f^*(x)| = |h_{\psi}(\hat{c}, y) - \Psi(y, c^*)| \leq \underbrace{|h_{\psi}(\hat{c}, y) - h_{\psi}(c^*, y)|}_{\text{perturb. in } c} + \underbrace{|h_{\psi}(c^*, y) - \Psi(y, c^*)|}_{\leq \delta_3}.$$

Using Lipschitzness of h_{ψ} in its first argument on $c^*(K)$, we obtain

$$\sup_{x \in K} |f_{\Theta}(x) - f^*(x)| \leq \text{Lip}_c(h_{\psi}) \sup_{x \in K} \|\hat{c} - c^*\| + \delta_3 \leq \text{Lip}_c(h_{\psi})(\text{Lip}(g_{\phi}) \delta_1 + \delta_2) + \delta_3.$$

Given $\varepsilon > 0$, choose $(\delta_1, \delta_2, \delta_3)$ so that the right-hand side is $< \varepsilon$ (e.g., split ε equally after estimating the Lipschitz constants, which are finite on compact sets). This proves the claim. \square

Assumption 1 (Optimization setting). Let $L(\Theta) = L_{\text{data}}(\Theta) + \lambda_{\text{phys}}(t) L_{\text{phys}}(\Theta) + \lambda_{\text{con}} L_{\text{con}}(\Theta) + \lambda_{\text{reg}} \|\Theta\|_2^2$. Assume: (i) $L_{\text{data}}, L_{\text{phys}}, L_{\text{con}}$ have L -Lipschitz gradients and are bounded below by 0; (ii) stochastic gradients g_t satisfy $\mathbb{E}[g_t | \Theta_t] = \nabla L(\Theta_t)$ and $\mathbb{E}\|g_t - \nabla L(\Theta_t)\|^2 \leq \sigma^2$; (iii) step sizes $\eta_t > 0$ obey $\sum_t \eta_t = \infty$, $\sum_t \eta_t^2 < \infty$; (iv) the ramp-up schedule $\lambda_{\text{phys}}(t)$ is nondecreasing and admissible in the sense that

$$\eta_t \lambda_{\text{phys}}(t) \rightarrow 0 \quad \text{and} \quad \sum_{t=0}^{\infty} \eta_t \lambda_{\text{phys}}(t) = \infty, \quad (23)$$

e.g., $\lambda_{\text{phys}}(t) = \lambda_0 \log^\beta(1+t)$ with $\beta \in (0, 1)$ and $\eta_t = \eta_0/t$.

Theorem 2 (SGD with Physics Ramp-up). Under Assumption 1, the SGD iterates satisfy

$$\lim_{\vartheta \rightarrow \infty} \mathbb{E}[\|\nabla L(\Theta_\vartheta)\|^2] = 0 \quad \text{and} \quad \lim_{t \rightarrow \infty} \mathbb{E}[L_{\text{phys}}(\Theta_\vartheta)] = 0.$$

Proof. We adapt the Robbins–Monro/Kushner–Yin analysis with a coupled potential.

Step 1 (expected descent of L). L is L -smooth for each fixed ϑ ; let $\Delta_\vartheta = \Theta_{\vartheta+1} - \Theta_\vartheta = -\eta_\vartheta g_\vartheta$. By smoothness and conditional unbiasedness,

$$\begin{aligned} \mathbb{E}[L(\Theta_{\vartheta+1}) | \Theta_\vartheta] &\leq L(\Theta_\vartheta) + \langle \nabla L(\Theta_\vartheta), \mathbb{E}[\Delta_\vartheta | \Theta_\vartheta] \rangle + \frac{L}{2} \mathbb{E}[\|\Delta_\vartheta\|^2 | \Theta_\vartheta] \\ &= L(\Theta_\vartheta) - \eta_\vartheta \|\nabla L(\Theta_\vartheta)\|^2 + \frac{L}{2} \eta_\vartheta^2 (\|\nabla L(\Theta_\vartheta)\|^2 + \sigma^2). \end{aligned}$$

Taking full expectation and rearranging yields

$$\mathbb{E}[L(\Theta_{\vartheta+1})] \leq \mathbb{E}[L(\Theta_\vartheta)] - \eta_\vartheta \left(1 - \frac{L}{2} \eta_\vartheta\right) \mathbb{E}\|\nabla L(\Theta_\vartheta)\|^2 + \frac{L}{2} \eta_\vartheta^2 \sigma^2. \quad (24)$$

Because $\sum_\vartheta \eta_\vartheta^2 < \infty$ and $L(\Theta_\vartheta) \geq 0$, summing equation (24) telescopically gives

$$\sum_{\vartheta=0}^{\infty} \eta_\vartheta \mathbb{E}\|\nabla L(\Theta_\vartheta)\|^2 < \infty,$$

hence $\liminf_{\vartheta \rightarrow \infty} \mathbb{E}\|\nabla L(\Theta_\vartheta)\|^2 = 0$. A standard Cesàro argument then upgrades \liminf to \lim .

Step 2 (vanishing physics violation). Consider the auxiliary potential $V_t = \mathbb{E}[L_{\text{phys}}(\Theta_t)]$. By L -smoothness of L_{phys} and the SGD step,

$$V_{\vartheta+1} \leq V_\vartheta - \eta_\vartheta \lambda_{\text{phys}}(\vartheta) \mathbb{E}[\|\nabla L_{\text{phys}}(\Theta_\vartheta)\|^2] + C_1 \eta_\vartheta \mathbb{E}[\langle \nabla L_{\text{phys}}, \nabla \tilde{L} \rangle] + C_2 \eta_\vartheta^2,$$

for some constants C_1, C_2 depending on the Lipschitz constants and gradient variance, and where $\tilde{L} = L_{\text{data}} + \lambda_{\text{con}} L_{\text{con}} + \lambda_{\text{reg}} \|\Theta\|_2^2$. Young's inequality absorbs the mixed inner product into $\frac{1}{2} \eta_\vartheta \lambda_{\text{phys}}(\vartheta) \|\nabla L_{\text{phys}}\|^2 + \frac{C_1^2}{2} \eta_\vartheta \lambda_{\text{phys}}(\vartheta)^{-1} \|\nabla \tilde{L}\|^2$. Taking expectations and summing yields the almost-supermartingale inequality

$$V_{\vartheta+1} \leq V_\vartheta - \frac{1}{2} \eta_\vartheta \lambda_{\text{phys}}(\vartheta) \mathbb{E}\|\nabla L_{\text{phys}}(\Theta_\vartheta)\|^2 + b_\vartheta, \quad \sum_{\vartheta=0}^{\infty} b_\vartheta < \infty, \quad (25)$$

where $b_\vartheta = C_2\eta_\vartheta^2 + \frac{C_1^2}{2}\eta_\vartheta\lambda_{\text{phys}}(\vartheta)^{-1}\mathbb{E}\|\nabla\tilde{L}(\Theta_\vartheta)\|^2$ and the latter is summable thanks to equation (24) and the admissibility condition $\eta_\vartheta\lambda_{\text{phys}}(\vartheta) \rightarrow 0$ (which implies $\eta_\vartheta\lambda_{\text{phys}}(\vartheta)^{-1}$ is eventually bounded). By the Robbins–Siegmund theorem, equation (25) implies V_ϑ converges and $\sum_\vartheta\eta_\vartheta\lambda_{\text{phys}}(\vartheta)\mathbb{E}\|\nabla L_{\text{phys}}(\Theta_\vartheta)\|^2 < \infty$. Using the second admissibility condition $\sum_\vartheta\eta_\vartheta\lambda_{\text{phys}}(\vartheta) = \infty$ forces

$$\liminf_{\vartheta \rightarrow \infty} \mathbb{E}\|\nabla L_{\text{phys}}(\Theta_\vartheta)\|^2 = 0.$$

Finally, the Polyak–Lojasiewicz-type inequality for nonnegative L_{phys} on compact sublevel sets (a consequence of gradient-dominated smooth objectives) yields $\mathbb{E}[L_{\text{phys}}(\Theta_\vartheta)] \rightarrow 0$.¹ \square

Admissible schedules. Condition (23) is mild and met by common ramps, e.g. logarithmic or sub-polynomial $\lambda_{\text{phys}}(\vartheta) = \lambda_0 \log^\beta(1 + \vartheta)$ with $\beta \in (0, 1)$ and $\eta_\vartheta = \eta_0/\vartheta$, for which $\eta_\vartheta\lambda_{\text{phys}}(\vartheta) \rightarrow 0$ while $\sum_\vartheta\eta_\vartheta\lambda_{\text{phys}}(\vartheta) = \infty$. In practice we employ a smooth version with saturation, but the analysis above captures the essential behaviour: physics pressure grows, yet the *effective* step $\eta_\vartheta\lambda_{\text{phys}}(\vartheta)$ vanishes, ensuring convergence while still driving the violation to zero.

F Extended Ablations and Sensitivity Studies

F.1 Complexity and runtime

The concept bottleneck and physics residuals add only a small overhead on top of the Transformer encoder. The encoder still dominates the cost with $\mathcal{O}(L^2d)$ attention, while the concept MLP and ODE head are $\mathcal{O}(dd_1 + d_1 \cdot 5)$ per step. Table 8 reports the training time per epoch and inference throughput on the ELECTRICITY dataset (horizon $H = 96$, batch size 64) on a single NVIDIA A100 GPU.

Table 8: Runtime comparison on ELECTRICITY. Training time per epoch and inference throughput (higher is better).

Method	Train time / epoch (s)	Inference throughput (sequences/s)
Informer	132	9.1k
FEDformer	165	7.4k
PatchTST	118	10.3k
TimeMixer	124	9.8k
DORIC (ours)	139	9.0k

DORIC is thus within 10–15% of recent baselines in both training and inference speed, showing that the concept–physics layer introduces only a modest computational overhead while providing substantial gains in accuracy and interpretability.

¹If a global PL condition is undesirable, one can instead argue by contradiction with compactness of $\{\Theta : L(\Theta) \leq L(\Theta_0)\}$: a nonvanishing limit of L_{phys} contradicts the accumulation of negative drifts in equation (25).

F.2 Robustness to Input Noise

We inject i.i.d. Gaussian noise with standard deviation $\sigma = 0.3 \hat{\sigma}_y$ into inputs at test time and report the MSE ratio relative to clean evaluation: $\text{ratio} = \text{MSE}_{\text{noisy}}/\text{MSE}_{\text{clean}}$.

Table 9: **30% additive Gaussian noise: MSE ratio** (lower is better; 1.00 means no change). For reference we also report averaged ratios for two strong baselines evaluated under the same protocol.

Model	Electricity	Traffic	Weather	Illness	Exchange	ETT	Avg.
DORIC	1.120	1.150	1.050	1.170	1.090	1.110	1.120
FEDformer (avg)	1.470	1.510	1.390	1.440	1.530	1.460	1.470
LogTrans (avg)	1.520	1.580	1.420	1.550	1.490	1.500	1.510

DORIC’s concept distributions exhibit a KL shift < 0.04 nats at $\sigma = 0.3 \hat{\sigma}_y$, indicating that the bottleneck geometry remains stable under heavy perturbation; physics residuals suppress noise-amplified accelerations.

F.3 Physics Ramp Schedule Study

Although the implementation uses $\lambda_{\text{phys}} = 1$ by default, we examine ramped variants that saturate at 1: *log-ramp* (default), *linear-10* (linear growth over 10 epochs), *cosine-10*, and a *step-10* schedule that switches from 0 to 1 at epoch 10. We report average MSE (96-step), epochs to reach mean squared violation $E[R_y^2] < 10^{-3}$, and training stability (std of train MSE).

Table 10: **Ramp schedule sweep.** Log-ramp gives the fastest feasibility with best stability; step-ramp delays feasibility and slightly worsens accuracy.

Schedule	Avg. MSE	Epochs to $E[R_y^2] < 10^{-3}$	Train MSE std.
log-ramp (default)	0.248	8.000	0.012
cosine-10	0.249	9.000	0.013
linear-10	0.251	10.000	0.014
step-10	0.262	16.000	0.019

F.4 Hyper-parameter Sensitivity

We probe look-back L , concept window τ , attention heads H , encoder depth N_L , and physics sampling budget $|S|$. All sweeps use the same data splits.

F.5 Per-Channel Physics Weights and Data Loss Variants

We compare a scalar λ_{phys} versus per-channel learned weights $\lambda_{\text{phys}}^{(j)}$. We also evaluate Huber and quantile losses as alternatives for L_{data} in heavy-tailed domains.

Table 11: **Sensitivity sweeps** (Avg. MSE at horizon 96). The default is bold. Larger L slightly helps periodic domains at the cost of latency; too small/large τ underfits/oversmooths concept statistics.

Setting	Avg. MSE	Setting	Avg. MSE	Setting	Avg. MSE
$L = 60$	0.261	$\tau = 10$	0.252	$H = 2$	0.251
$L = 120$	0.248	$\tau = 25$	0.248	$H = 4$	0.248
$L = 168$	0.246	$\tau = 50$	0.251	$H = 8$	0.249
$N_L = 1$	0.250	$ S = 16$	0.251	$ S = 64$	0.248
$N_L = 2$	0.248	$ S = 256$	0.248		

Table 12: **Per-channel physics weighting and loss variants**. Per-channel weights reduce amplitude shrinkage on soft-law variables (Weather). Robust data losses slightly improve heavy-tailed spikes (Electricity) without harming other domains.

Variant	Avg.	Elec.	Traffic	Weather	Illness	FX	ETT
Scalar $\lambda_{\text{phys}}=1$ (default)	0.248	0.138	0.313	0.007	0.869	0.051	0.111
Per-channel $\lambda_{\text{phys}}^{(j)}$	0.247	0.137	0.312	0.007	0.867	0.051	0.111
Huber $L_{\delta=1.0}$ for L_{data}	0.246	0.134	0.309	0.007	0.866	0.051	0.111
Quantile ($\tau=0.5$) for L_{data}	0.247	0.136	0.311	0.007	0.865	0.052	0.112

Takeaways. (1) Per-channel physics avoids over-penalizing soft-law channels (humidity) while keeping the global inductive bias. (2) Robust L_{data} choices (Huber/quantile) mitigate outlier-driven spikes (Electricity) and can be used as drop-in replacements when heavy tails dominate.

F.6 Checks Against Theory

Across all sweeps, we consistently observe: (i) early collapse of physics violation (feasibility), followed by (ii) steady decrease in concept misalignment (identifiable geometry), and (iii) monotone improvement of data fit (approximation within the feasible manifold)—a pattern predicted by the universal expressiveness and ramp-up convergence results.